

Efficient electroreduction of CO₂ to CO on silver single-atom catalysts: Activity enhancement through coordinated modulation of polyaniline

Teng Zhang ^a, Xingyu Lu ^{b,c}, Wei Qi ^{b,c,*}, Gaowu Qin ^{a,d}, Song Li ^{a,**}

^a Key Lab for Anisotropy and Texture of Materials (MoE), School of Material Science and Engineering, Northeastern University, Shenyang 110819, China

^b Shenyang National Laboratory for Materials Science, Institute of Metal Research, Chinese Academy of Sciences, Shenyang 110016, China

^c School of Materials Science and Engineering, University of Science and Technology of China, Shenyang 110016, China

^d Institute for Materials Intelligent Technology, Liaoning Academy of Materials, Shenyang 110010, China



ARTICLE INFO

Keywords:

Silver single atom
Polyaniline
Self-supported electrodes
Electrochemical CO₂ reduction to CO

ABSTRACT

The electrochemical reduction of CO₂ to CO is considered to be one of the most mature routes that could be commercialized for efficient utilization of large amount of CO₂. Silver (Ag) has shown high selectivity towards CO but usually requires high reduction potential. Herein, a novel Ag single atom-polyaniline (PANI) is constructed directly on gas diffusion electrode (GDE). The amino group with strong electron-donating ability in PANI can effectively promote the adsorption and activation of CO₂. In addition, the adsorption of *COOH is significantly enhanced on N-coordinated Ag. The proposed catalyst electrode shows an outstanding performance with the Faraday efficiency of CO close to 100% at -0.75 V (vs. RHE), the energy efficiency is 12.8% and the output of CO is 108.7 mL cm⁻² h⁻¹, which exceeds most state-in-art Ag-based catalysts, highlighting the importance for the rational design and controllable fabrication of active sites and their favorable chemical environments.

1. Introduction

Excessive carbon dioxide (CO₂) in atmosphere is one of the most aggravating global climate problems leading to disastrous consequences, such as the greenhouse effect and sea level rising etc. There is an urgent demanding to reduce CO₂ emissions and develop mature CO₂ capture, storage and conversion technologies to meet the strict environmental requirements [1,2]. Developing an artificial carbon cycle that could convert CO₂ into value-added chemicals and fuels, bringing economic benefits while reducing the concentration of CO₂ in the atmosphere, has received considerable attention in the research fields of catalysis, energy and material sciences [3–5]. The electrocatalytic carbon dioxide reduction reaction (eCO₂RR) exhibits unique advantages for efficient conversion and utilization of CO₂ comparing with other conventional technologies (eg. thermal catalysis and enzyme catalysis), since it can be carried out under ambient temperature and pressure using electricity from clean energy resources such as wind and solar energy etc [6].

Carbon monoxide (CO) is one of the main target product due to its

large industrial market needs and affordable electron-normalized prices, and eCO₂RR via the two-electron transfer reaction forming CO is considered as one of the most mature and feasible routes that has great potential to be commercialized comparing with other various products [7,8]. However, the efficiency of electrocatalytic CO₂RR to CO is still unsatisfactory due to the high energy barrier of CO₂ activation and the serious competition of hydrogen evolution reactions. Silver-based catalysts are considered as one of the most mature state-in-art catalysts, which typically exhibit high catalytic selectivity towards CO, but they normally suffer from low activity and a relatively high cathodic potential (e.g., ≥ -0.9 V vs. RHE) [9]. Therefore, the key scientific challenge for the practical implementation of eCO₂RR to CO is the development of efficient electrocatalysts with high activity and energy efficiency.

Introduction of conductive polymer into the electrocatalyst system can effectively adjust the chemical micro-environment and electronic structure of the metallic catalytic centers via the controllable chemical interactions between these two components, thereby improving the eCO₂RR efficiency of the catalyst [10–13]. For instance, it has been reported the successful construction of a polyaniline (PANI) shell on gold

* Corresponding author at: Shenyang National Laboratory for Materials Science, Institute of Metal Research, Chinese Academy of Sciences, Shenyang 110016, China.

** Corresponding author.

E-mail addresses: wqi@imr.ac.cn (W. Qi), lis@atm.neu.edu.cn (S. Li).

nanostructures, and the obtained gold/PANI nanocomposite exhibits an Faraday efficiency (FE) increase of ~40% to CO comparing with that of bare gold nanoparticles [14]. Zhuang and co-workers have coated the copper surface with a 50 nm thick PANI layer, and the catalyst exhibits an improvement of the FE_{CO} by 45% at -1.1 V (vs. RHE) [15]. The amine group with strong electron donating ability in PANI can effectively reduce the activation energy of CO_2 via binding to highly selective metal active sites. However, modification of metal electrocatalyst with PANI proceeds through post-treatment that will result in the excessive coverage of metal sites and in turn reduces their accessibility. Rational design of PANI-metal catalysts that enhances the activity of metal sites via electronic/coordinated modulation with full exposure of active sites to improve the reaction efficiency remains a key scientific challenge in this field, and the in-depth understandings on the catalytic reaction mechanism and structure-function relations is the ideal path to achieve this ultimate goal.

Herein, we have designed and fabricated a novel PANI-Ag single atom (Ag_{SA}) catalysts for highly efficient e CO_2 RR process producing CO as main product. The PANI nanocone arrays are directly constructed on the catalyst layer side of the commercial gas diffusion electrode (GDE) via in situ polymerization, and then Ag single atoms are loaded on PANI surface via simple impregnation method. The design of the GDE-PANI- Ag_{SA} self-supporting electrode would greatly expose the Ag single-atom active sites. The amino groups in PANI can quickly adsorb and activate CO_2 and convert it efficiently to CO on Ag site. The GDE-PANI- Ag_{SA} can readily afford a superb FE_{CO} of ~100% at a relatively low potential of -0.75 V (vs. RHE) in 1 M KOH using a flow cell, indicating the superiority of the proposed GDE-PANI- Ag_{SA} material comparing with other typical reported electrocatalysts, which lays an important theoretical foundation for the efficient utilization of CO_2 .

2. Experimental

2.1. Materials

Aniline (AN, $\text{C}_6\text{H}_7\text{N}$), ammonium persulfate (APS, $(\text{NH}_4)_2\text{S}_2\text{O}_8$), silver nitrate (AgNO_3), nitric acid (HNO_3) and potassium hydroxide (KOH) were purchased from Aladdin Bio-Chem Technology Co., Ltd. GDE was purchased from Shanghai Chuxi Industrial Co., Ltd. All chemicals were of analytical grade and were used without further purification.

2.2. Material synthesis

PANI nanocone arrays were vertically grown on GDE by in-situ polymerization of AN. The GDE consists of two layer sides: ultra-hydrophobic layer and catalyst layer. The ultra-hydrophobic layer was covered with a transparent tape before the polymerization experiment to avoid damaging. Typically, GDE was soaked in deionized water (20 mL) containing AN (0.04 M) at -5°C for 24 h. The same volume pre-cooled aqueous solution containing APS (0.01 M) was added to the reaction system. The GDE-PANI was obtained after reaction at -5°C for 24 h. To prepare GDE-PANI- Ag_{SA} , the synthesized GDE-PANI was immersed into AgNO_3 solution (20 mL, 0.04 M) for 12 h. Finally, the sample was washed with ethanol and deionized water. GDE-PANI- Ag_{SA} was obtained after washing and freeze drying. For comparison, the pH value of the solution during the preparation of PANI could be adjusted by HNO_3 , and the obtained samples were represented as PANI₁ to PANI₇. In addition, the molar ratio of AN to AgNO_3 (10:1, 5:1, 1:1, 5:1, 10:1) could also be tuned by changing the amount of AgNO_3 . In order to obtain GDE-Ag, the GDE was immersed into AgNO_3 solution (20 mL, 0.04 M) for 12 h, and the silver ions were in situ reduced during the e CO_2 RR process.

2.3. Characterizations

The morphologies of catalysts were observed on a JEOL JEM-2100 F

field emission scanning electron microscope (SEM) operated at an acceleration voltage of 30 kV and a JEOL JEM-ARM200F transmission electron microscope (TEM) at 200 kV. X-ray diffraction patterns (XRD) were recorded on a Rigaku-D/max 2500 V X-ray powder diffractometer using Cu K α radiation ($\lambda=1.5418 \text{ \AA}$). The X-ray photoelectron spectroscopy (XPS) analysis was performed on Themo ESCALAB 250 electron spectrometer using Al K α X-ray. Fourier transform infrared (FT-IR) spectra were obtained on a Themo Fisher Nicolet iS10 FT-IR system. The Raman experiments were measured on a HORIBA LabRam HR800 Raman spectrometer equipped with a laser source at a wavelength of 532 nm. X-ray absorption fine structure (XAFS) data was collected at BL16U1 beamline in Shanghai Synchrotron Radiation Facility (SSRF). The storage ring of SSRF was operated at 3.5 GeV with a maximum current of 240 mA. Using a Si (111) double-crystal monochromator, the GDE-PANI- Ag_{SA} data of the catalyst was measured in fluorescence mode with a solid-state detector. Ag foil and Ag_2O K-edge data of the catalyst were carried out in transmission mode for energy calibration. All spectra were collected in ambient conditions.

2.4. Electrochemical measurements

Electrochemical measurements were conducted in an electrochemical flow cell which including a gas chamber, a cathodic chamber, and an anodic chamber. An anion exchange membrane was used to separate the anodic and cathodic chambers. A Pt plate was used as the counter electrode and Ag/AgCl as the reference electrode. 1 M KOH solution was used as the electrolyte and circulated to the anode and cathode chambers at a constant flow rate of 10 mL min $^{-1}$. The flow rate of CO_2 gas through the gas chamber was controlled to 20 sccm using a digital gas flow controller. Linear sweep voltammetry (LSV) curves were obtained by scanning the potential at the rate of 5 mV s $^{-1}$. Fourier-transformed alternating current voltammetry (FTacV) was carried out with an amplitude of 80 mV and a frequency of 9.02 Hz. Double layer capacitance was obtained by cyclic voltammetry (CV) recorded within a potential range from -0.03 V to -0.13 V (vs. RHE) at the scan rate from 20 to 120 mV s $^{-1}$. The CV tests were performed in a single cell with three electrodes, and a 0.5 M KHCO_3 solution was applied as the electrolyte. Electrochemical impedance spectroscopy (EIS) was conducted to determine the total uncompensated resistance. Potential waveforms were applied to the flow cell with an amplitude of 5 mV of 10 MHz to 100 kHz. The OH^- adsorption reaction was carried out in a single three-electrode electrochemical cell and conducted in argon-saturated 0.1 M KOH with a 10 mV s $^{-1}$ scan rate.

2.5. Product analysis

The gaseous product of electrochemical experiments was directly introduced into the gas chromatograph (Agilent 7890 A GC System), which was equipped with thermal conductivity detector (TCD) and flame ionization detector (FID) detector. The liquid products were detected by 1 H NMR (BRUKER AVANCEAV III HD 500). The FE was calculated using the following equation:

$$\text{FE}_g = \frac{V_g v n F P}{R T j}$$

where V_g is the volume concentration of gas products detected by GC, v the flow rate of CO_2 , n the number of electrons transferred to CO_2 to produce a given product, F the faraday constant (96,485 C mol $^{-1}$), P the pressure (101,325 Pa), R the gas constant (8.314 J mol $^{-1}$ K $^{-1}$), T the temperature for testing, and j the current density.

$$\text{FE}_l = \frac{C_l V n F}{t j}$$

where C_l is the concentration of the liquid product determined using NMR (mol L $^{-1}$), V the volume of the catholyte, and t the reaction time.

The formation rate (R) for each species were calculated using the following equation:

$$R = \frac{Q \times FE}{F \times n \times t \times S}$$

where Q is the total charge and S is the geometric area of the electrode (cm^2).

3. Results and discussions

As shown in Fig. 1a, PANI could be vertically grown on GDE via in situ polymerization of aniline (AN) monomers to obtain GDE-PANI, and then Ag single atoms were synthesized and anchored on PANI surface via reduction of aqueous Ag^+ precursors under mild reaction conditions. The SEM and TEM images in Figs. 1b-d and S1-S4 showed that PANI nano-cone arrays were successfully grown on the surface of GDE in the obtained GDE-PANI- Ag_{SA} composite electrode. The dispersion state of Ag species on PANI was further confirmed by aberration-corrected high-angle annular dark-field scanning transmission electron microscopy (HAADF-STEM) (Fig. 1e). The uniformly dispersed high-density bright dots corresponded to Ag single atoms on the PANI surface [16]. Notably, no apparent Ag nanoparticles or nanoclusters could be observed on PANI surface in the whole region of the HAADF-STEM images (Fig. 1f). Energy-dispersive spectroscopy (EDS) mapping images also revealed the homogeneous distributions of C, N, Ag over the PANI surface.

The chemical composition and structure of GDE-PANI- Ag_{SA} were

further revealed via multiple characterization techniques. As shown in Fig. 2a, only two peaks centered at 26.2° and 54.3° could be observed in XRD patterns, which were assigned as the (002) and (004) planes of carbon, suggesting the absence of metal aggregates. As shown in Fig. 2b, the characteristic FT-IR peaks belonging to PANI and Ag (at 486 cm^{-1}) [17,18] indicated the successful synthetic procedure. It could be observed that the characteristic peaks belonging to PANI shifted to lower wavenumbers with higher intensity in PANI- Ag_{SA} than in pure PANI, indicating the structural change of PANI after introducing Ag. Ag single atom might have strong interactions with N sites in PANI.

XPS and XAFS were also conducted to further determine the electronic structure and coordination environment of Ag single atom species in GDE-PANI- Ag_{SA} . XPS survey spectra exhibited the binding energy signals belonging to C 1 s, Ag 3d, N 1 s and O 1 s (Fig. S5). The detailed deconvolution of N 1 s XPS spectra was shown in Fig. 2c, and $-\text{N}=$ (quinoid units) and $-\text{NH}-$ (benzenoid units) were proved as the major nitrogen species in PANI [14]. The N 1 s signal shifted to higher binding energy position after Ag was introduced to form Ag-N bond, further suggesting the relatively strong interactions and related electron transfer process between N and Ag species, which might be conducive to the electroreduction of CO_2 . As shown in Fig. 2d, the binding energies of the Ag 3d_{3/2} and Ag 3d_{5/2} peaks located at 374.18 eV and 368.06 eV, respectively, suggesting that the valence state of Ag is between 0 and +1 [19], and the content of Ag was estimated at around 1 at% (Table S1). The normalized Ag K-edge absorption spectra in Fig. 2e further confirmed that Ag species in GDE-PANI- Ag_{SA} existed in the partially

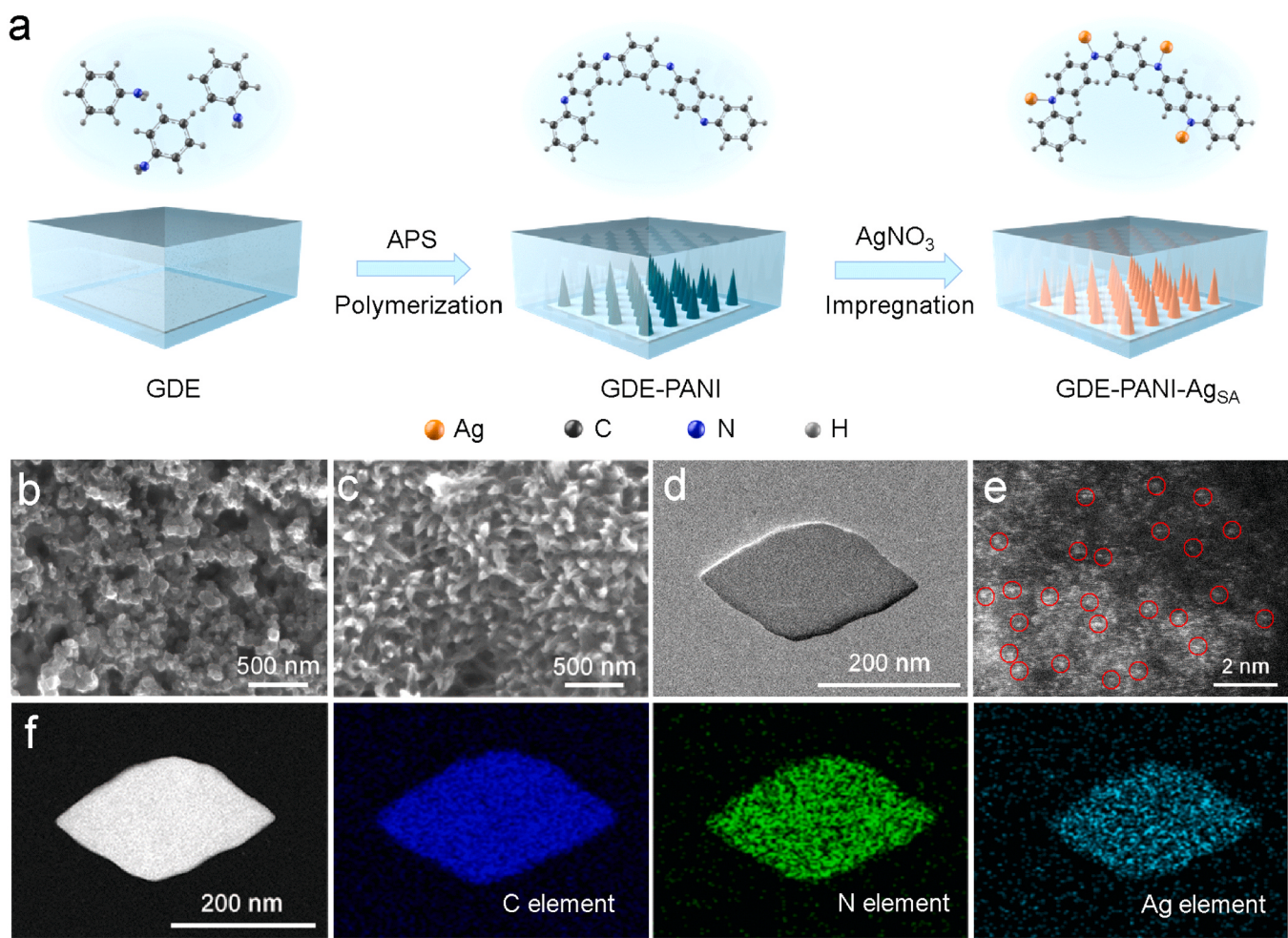


Fig. 1. Workflow for the fabrication procedure and morphology of GDE-PANI- Ag_{SA} . (a) Schematic illustration for construction of GDE-PANI- Ag_{SA} electrocatalyst. (b, c) SEM images of GDE and GDE-PANI- Ag_{SA} . (d) TEM image of PANI- Ag_{SA} . (e) Aberration-corrected HAADF-STEM image of PANI- Ag_{SA} . (f) HAADF-STEM image of PANI- Ag_{SA} and EDS element distribution of C, N, and Ag.

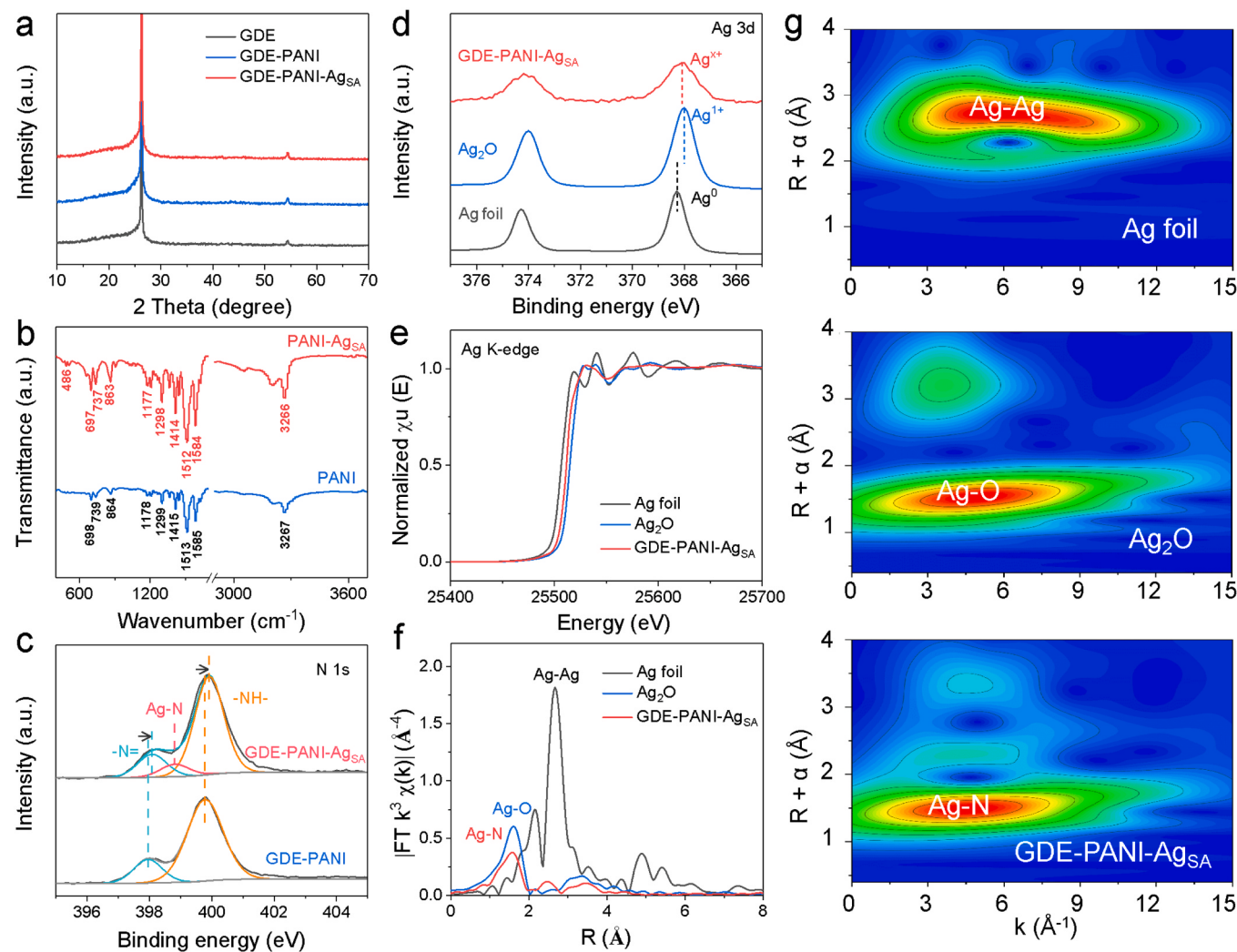


Fig. 2. Structural characterization of GDE-PANI-Ag_{SA}. (a) XRD patterns. (b) FT-IR spectra. (c, d) N 1 s and Ag 3d XPS spectra. (e) XANES spectra of Ag K-edge. (f) FTs of K³-weighted Ag K-edge EXAFS data. (g) Wavelet-transform EXAFS analysis with high resolution in both R- and k-spaces was also carried out to reveal the structural information of GDE-PANI-Ag_{SA} (Fig. 2g). Unlike the Ag-Ag bond (6.4 \AA^{-1}) in Ag foil and Ag-O bond (4.9 \AA^{-1}) in Ag₂O [21], the Ag-N bond with the maximum intensity at about 4.5 \AA^{-1} was detected in PANI-Ag, which further confirmed the atomic dispersion of Ag in GDE-PANI-Ag_{SA}, and the dominant active sites in GDE-PANI-Ag might be AgN₄ coordination species.

The CO₂ electroreduction performance of the samples were evaluated in 1 M KOH using a flow cell system with typical gas diffusion electrode (GDE). The reversible hydrogen electrode (RHE) was used as the reference for all potentials, and the ohmic potential drop loss caused by electrolyte resistance was subtracted. As shown in the polarization curves (Fig. S7), the GDE-PANI-Ag_{SA} catalyst demonstrated the highest current density comparing with GDE-PANI and GDE-Ag_{SA}. To evaluate, identify and optimize the interactions between PANI and Ag, a series of samples for control experiments were prepared, in which PANI was synthesized in different pH solutions (pH=1–7) or different molar ratios of AN:Ag (10:1, 5:1, 1:1, 1:5, 1:10). The GDE-PANI-Ag_{SA} sample, in which PANI was prepared in neutral solution (pH=7) and the molar ratio of AN:Ag was controlled at 1:1, showed the best activity suggesting this sample may have more active sites. Although the PANI prepared in a strong acidic solution can improve its conductivity, the amino group ($-\text{NH}-$) will be oxidized as shown in its FT-IR spectra (Fig. S8) leading to its limited CO₂RR activity. In addition, the XPS results of these series of GDE-PANI-Ag_{SA} samples (GDE-PANI₂-Ag_{SA} to GDE-PANI₇-Ag_{SA}) indicated that the N 1 s signal shifted to higher binding energy position with increase of the pH value from pH=2 to pH=7 in the preparation procedure, which further suggested that the interactions between the $-\text{NH}-$ and Ag got stronger in the GDE-PANI-Ag_{SA} sample prepared under neutral condition (Fig. S9). These above results indicated that $-\text{NH}-$ sites may be the key factor to activate CO₂ [22]. In addition, lower Ag content would lead to insufficient catalytic activity, and too much Ag species may cover the $-\text{NH}-$ sites on the catalyst surface, which would also lead to a lower CO₂ activation capacity.

The selectivity and the corresponding Faradic Efficiency (FE) values

of all catalysts in CO₂RR were quantified by a series of controlled-potential electrolysis experiments (Fig. S10). Only CO and slight amount of H₂ could be detected under the catalysis of all these samples. The optimized GDE-PANI-Ag_{SA} catalyst exhibited relatively high FE_{CO} close to 100% at -0.75 V (vs. RHE), outperforming GDE-PANI (21.11%) and GDE-Ag_{SA} (53.53%) (Fig. 3a) and GDE-PANI-Ag_{SA} catalysts with other different molar ratio of AN to Ag (1:10–75.24%, 1:5–85.66%, 5:1–65.89%, 10:1–54.39%) (Fig. 3b), which also suggested that the interactions between single atom Ag and PANI might promote the electroreduction of CO₂ to produce CO, and the loading of Ag content should be moderate to ensure the high selectivity and activity. In addition, the FE_{CO} of the sample with PANI prepared in neutral solution increased by about 15% comparing with that PANI prepared in acid solution, further demonstrating the contribution of -NH- group to CO₂RR activity (Fig. 3c). The energy efficiency (EE), which is defined as: EE=E^θ×FE/E^θ+η (E^θ and η represents thermodynamic equilibrium potential and overpotential, respectively), of the proposed CO₂RR system was calculated at 12.8% when the Faraday efficiency of CO close to 100% at -0.75 V vs. RHE.

As shown in Fig. S11, the partial current density of CO (j_{CO}) for GDE-PANI-Ag_{SA} catalyst was higher than that for all the other samples, which further manifested that the superior CO₂RR electrocatalytic activity of GDE-PANI-Ag_{SA} towards CO should be attributable to the coexistence and proper content of PANI and Ag components. Meanwhile, the FE_{CO} of

GDE-PANI-Ag decreased gradually with the increasing of the current density (from -100 to -400 mA cm⁻²) as shown in Fig. 3d. The partial current density of CO reached its maximum (-231.4 mA cm⁻²) at -300 mA cm⁻² (Fig. 3e). The GDE-PANI-Ag_{SA} sample had shown the highest electrochemical double-layer capacitance (Figs. S12–14) and the smallest charge transfer resistance (Fig. S15), suggesting that it had the most abundant active sites and electron transfer ability.

Fig. 3f showed the relationship of the formation rate of CO as a function of the current density for all the catalysts. The formation rate of CO for GDE-PANI-Ag_{SA} was observed as high as 4500.7 μmol cm⁻² h⁻¹ under the current density of -300 mA cm⁻², and the output of CO reached 108.7 mL cm⁻² h⁻¹. The output is critical for industrial employment [23]. The relatively high FE_{CO} could be maintained over 90% at the constant potential of -0.75 V (vs. RHE) or over 75% at the constant current density of -300 mA cm⁻² within 10 h as shown in Fig. 3g and Fig. 3h, respectively, suggesting the high stability of GDE-PANI-Ag_{SA}. The FT-IR spectra of GDE-PANI-Ag_{SA} after long-term stability test exhibited the well-maintained structure of the catalyst as shown in Fig. S16, and the slight decrease of the FT-IR peak intensity might be due to the degradation of PANI caused by the reduction process under high potential for a relatively long period, which also led to the gradual decrease of the current density. The well-designed and optimized GDE-PANI-Ag_{SA} catalyst achieved high FE_{CO} at relatively low reaction potential, which outperformed most reported state-in-art

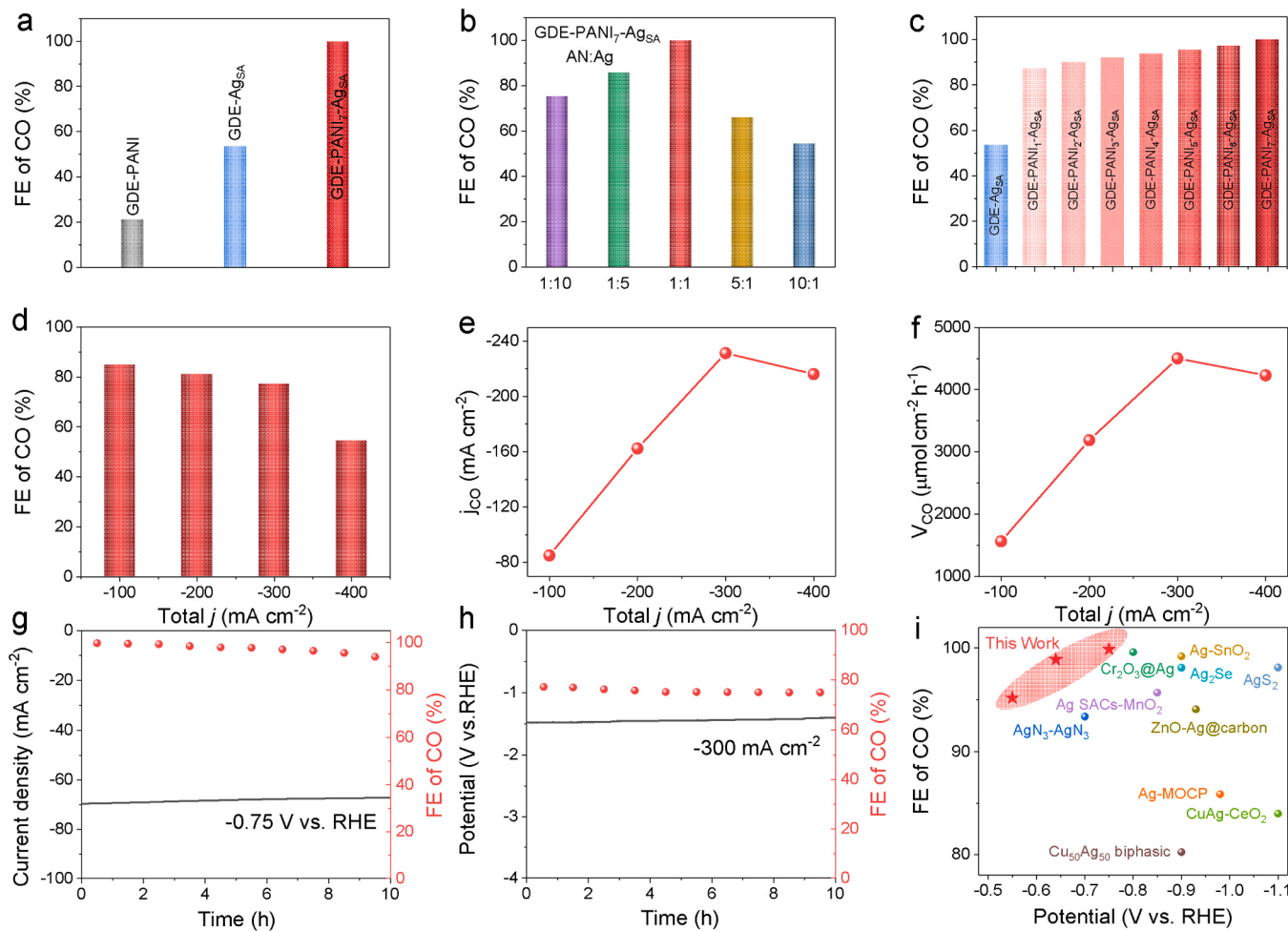


Fig. 3. Electrochemical CO₂ reduction performance in a flow cell system. (a) Maximum FE_{CO} of GDE-PANI, GDE-Ag_{SA} and GDE-PANI-Ag_{SA} at -0.99, -0.96, -0.75 V (vs. RHE), respectively. (b) Maximum FE_{CO} of GDE-PANI-Ag_{SA} with different molar ratios of AN:Ag (1:10, 1:5, 1:1, 5:1, 10:1). (c) Maximum FE_{CO} of GDE-Ag_{SA}, GDE-PANI₁-Ag_{SA}, GDE-PANI₂-Ag_{SA}, GDE-PANI₃-Ag_{SA}, GDE-PANI₄-Ag_{SA}, GDE-PANI₅-Ag_{SA}, GDE-PANI₆-Ag_{SA} and GDE-PANI₇-Ag_{SA} at AN:Ag = 1:1. (d-f) FE, partial current density and formation rates of CO for GDE-PANI₇-Ag_{SA} under different applied current densities. (g) Stability test at -0.75 V (vs. RHE) for GDE-PANI₇-Ag_{SA}. (h) Stability test at -300 mA cm⁻² for GDE-PANI₇-Ag_{SA}. (i) Maximum FE_{CO} as a function of potential for GDE-PANI-Ag_{SA} in comparison with other literature reports.

Ag-based electrochemical CO₂RR catalysts (Fig. 3i) from the viewpoint of both Faraday Efficiency and overpotential [24–33], suggesting its unique advantage and potential in practical applications.

To further demonstrate the advantages of the proposed self-supported GDE-PANI-Ag_{SA} electrode catalyst, we had prepared a series of control samples with different structure, namely PANI growing on GDE-Ag_{SA} (GDE-Ag_{SA}-PANI), Ag single atoms growing on GDE-nitrogen doped carbon (GDE-NC-Ag_{SA}) and PANI-Ag_{SA} powder electrode. The FE_{CO} of GDE-Ag_{SA}-PANI (60.52%) was observed obviously lower than that of GDE-PANI-Ag_{SA} (~100%) under the same reaction conditions due to the coverage of PANI on the Ag active sites (Fig. S17). The GDE-PANI-Ag_{SA} after calcination at 900 °C (GDE-NC-Ag_{SA}) exhibited only limited selectivity (2.7% at -0.97 V vs. RHE) towards CO due to the destruction of the coordination environment of Ag single atom after high temperature thermal treatment (Fig. S18). In addition, the performance of the PANI-Ag_{SA} powder electrode (89.8% at -0.89 V vs. RHE) was also observed inferior to that of the GDE-PANI-Ag self-supported electrode (Fig. S19). This phenomenon suggested that the vertical array morphology might also facilitate the exposure of more active sites than the horizontal dispersion of the powder sprayed on GDE in addition to the obvious advantages in avoiding the use of binders in the electrode, illustrating the superiority of GDE-PANI-Ag_{SA} in structural design.

Fourier-transformed alternating current voltammetry (FTacV) could supplement the deficiencies of direct current voltammetry measurements, providing comprehensive information by suppressing

background current during the catalytic reaction process [34,35]. Therefore, the onset potential could be accurately measured by comparing the FTacV data from the reduction reaction in Ar or CO₂ atmosphere at the lower potential range (0~−0.5 V vs. RHE), in which region CO₂RR is the dominant reaction rather than hydrogen evolution reaction. It could be observed from the third harmonic components of the FTacV (Fig. 4a) that the onset potential of GDE-PANI-Ag_{SA} was determined at around -0.2 V (vs. RHE). However, the current change can not be detected for GDE-PANI and GDE-Ag_{SA} in the same potential range, indicating that these catalysts are not thermodynamically conducive to the CO₂ electroreduction reaction, which further demonstrated the superior CO₂RR catalytic activity of GDE-PANI-Ag_{SA}.

Tafel slope measurements were used to provide profound insights into the fundamental CO₂RR kinetics and reaction mechanism. The theoretical Tafel slopes for the activation and surface reaction of CO₂ were estimated to be 118 and 59 mV dec⁻¹, respectively [36]. As shown in Fig. 4b, GDE-PANI-Ag_{SA} exhibited a Tafel slope of 103 mV dec⁻¹, which is much lower than those obtained from GDE-PANI (391 mV dec⁻¹) and GDE-Ag_{SA} (307 mV dec⁻¹), indicating the favorable kinetics of GDE-PANI-Ag_{SA} for the electrocatalytic reduction of CO₂ to CO. The improvement of electrocatalytic CO₂RR kinetics on GDE-PANI-Ag_{SA} might be attributed to the enhanced adsorption of CO₂ by PANI carrier.

It is known that the formation and stabilization of CO₂^{•−}/*COOH intermediates would be a key factor to determine the intrinsic electrocatalytic activity of the electrode [37]. The formation of *COOH also

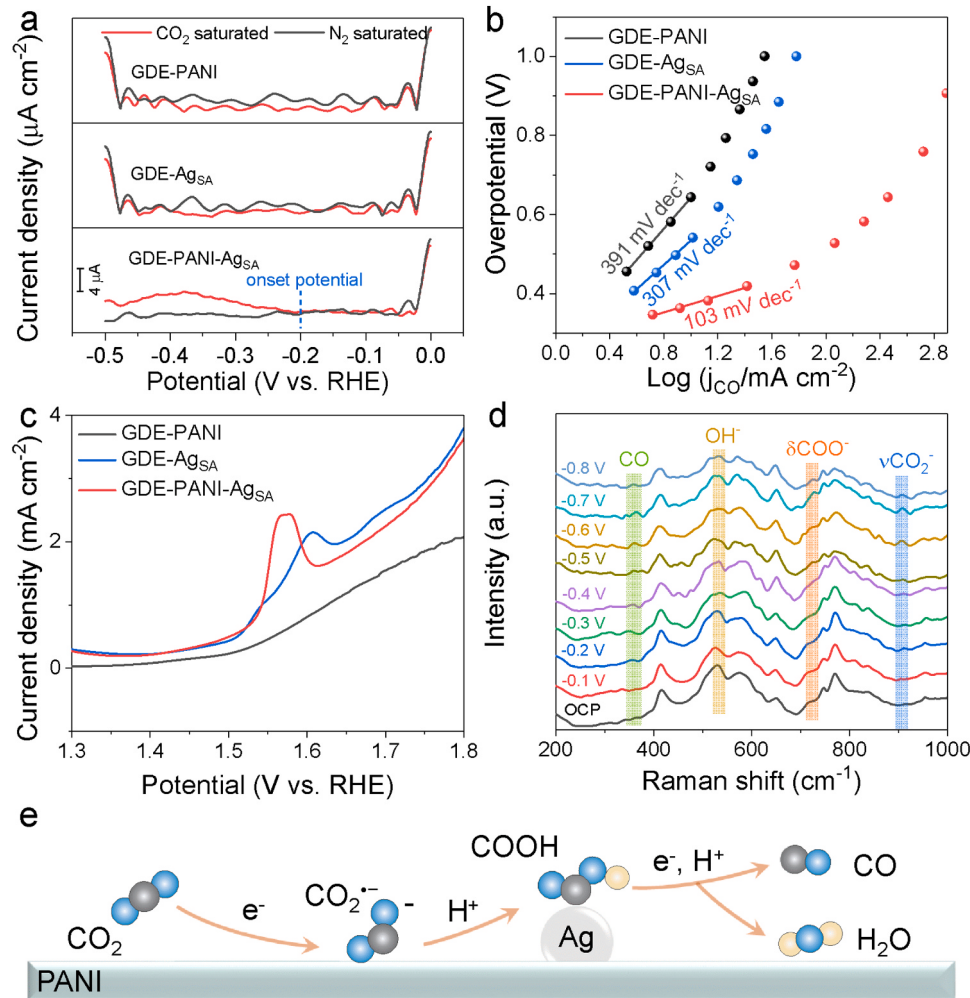


Fig. 4. (a) Third harmonic components of FTacV for GDE-PANI, GDE-Ag_{SA} and GDE-PANI-Ag_{SA}. (b) Tafel plots of GDE-PANI, GDE-Ag_{SA} and GDE-PANI-Ag_{SA}. (c) LSV curves of GDE-PANI, GDE-Ag_{SA} and GDE-PANI-Ag_{SA} in Ar-saturated 0.1 M KOH solution at a scan rate of 10 mV s⁻¹. (d) In situ Raman spectra of GDE-PANI-Ag_{SA} at various potentials (vs RHE) during CO₂RR. (e) Reaction steps for the electroreduction of CO₂ to CO on GDE-PANI-Ag_{SA} catalysts.

depended on the ability of the catalyst surface to adsorb OH^- , and in that case the electrochemical adsorption of OH^- on the proposed catalysts were further investigated via LSV measurements (Fig. 4c). The OH^- adsorption peak on GDE-Ag_{SA} appeared at 1.61 V (vs. RHE), while this peak on GDE-PANI-Ag_{SA} catalyst was cathodically shifted to 1.57 V (vs. RHE), confirming a stronger adsorption strength of GDE-PANI-Ag_{SA} towards OH^- , and thus the reaction potential could be effectively lowered. Subsequently, the increased concentration of $\text{CO}_2^-*/\text{COOH}$ on the catalyst surface promoted the formation of CO. The reaction process can be monitored and observed directly via *in situ* Raman spectra to detect the reaction intermediates (Figs. 4d, S20). The characteristic peaks observed under open circuit potential (OCP) conditions were all attributed to PANI. With the gradual increase of potential, new peaks appeared at 358 cm^{-1} , 534 cm^{-1} , 724 cm^{-1} and 910 cm^{-1} were related to the vibration signal of CO, OH⁻, δCOO^- and νCO_2^- [38–40]. These species were considered as the key intermediates for CO production, and no other species could be detected, which also proved that GDE-PANI-Ag_{SA} catalyst was highly selective to CO. The CO_2^- species could be formed under a very small cathode potential (-0.1 V vs. RHE), indicating that GDE-PANI-Ag_{SA} had a strong ability to activate CO_2 . Fig. 4e showed the reaction steps from CO_2 to CO. PANI dominates the activation of CO_2 , accelerating the kinetic process of CO_2 on the Ag surface, resulting in the rapid conversion of CO_2 to CO on GDE-PANI-Ag_{SA}.

In a word, the improvement of CO_2 electroreduction activity and CO selectivity should be attributed to the coexistence of PANI and Ag single atom. In order to analyze the physical chemical nature behind the enhancement of CO_2RR activity from PANI, the following experiments were designed and conducted. The adsorption capacity and strength of CO_2 on the electrode catalysts are crucial for reducing the energy barrier

of CO_2 reduction. It could be found in the CO_2 adsorption isotherms (Fig. 5a) that the adsorption capacity towards CO_2 of GDE-PANI-Ag_{SA} increased by ~48% comparing with GDE-Ag_{SA}. Simultaneously, the temperature-programmed desorption (TPD) profiles of CO_2 showed that GDE-PANI-Ag_{SA} exhibited higher CO_2 adsorption strength than GDE-PANI and GDE-Ag_{SA} (Fig. 5b). The relatively high desorption temperature indicated that chemical adsorption was the main form for CO_2 adsorption on GDE-Ag_{SA} and GDE-PANI-Ag_{SA}. Our calculated CO_2 adsorption energies are generally consistent with the estimates from TPD spectra obtained by using the Redhead equation [41,42], which is defined as: $E_{\text{des}} = RT_{\text{max}}[\ln(vT_{\text{max}}/\beta) - 3.64]$ (E_{des} is the activation energy of desorption, R is the gas constant, T_{max} is the peak maximum temperature, v is the pre-exponential factor and β is the heating rate dT/dt). With CO_2 adsorption peak temperature at 329 and 206°C on GDE-PANI-Ag_{SA} and GDE-Ag_{SA}, the adsorption energies are estimated to be 63.67 and 102.94 kJ/mol, proving that the adsorption energy of CO_2 was significantly improved after Ag coordinated with $-\text{HN}-$ in PANI. The enrichment of CO_2 on the GDE-PANI-Ag_{SA} electrode should be attributed to the specific interactions between the $-\text{NH}-$ groups in PANI and CO_2 molecules, which might benefit the CO_2RR process significantly. Comparing with pure PANI, the CO_2 -treated PANI showed an additional characteristic peak attributed to the formation of $-\text{HN}-\text{CO}_2$ at 1099 cm^{-1} in the FT-IR spectra (Fig. 5c), indicating the strong interactions between the amino group from PANI and CO_2 [43]. In addition, it could be observed that the current density for hydrogen evolution reaction (HER) on GDE-PANI-Ag_{SA} catalyst was significantly lower than that on GDE-Ag_{SA} (Fig. 5d), indicating the effect of PANI for inhibiting HER process via enrichment of CO_2 . Based on all these results, it can be concluded that PANI-Ag_{SA} synergistically enhance the FE of CO

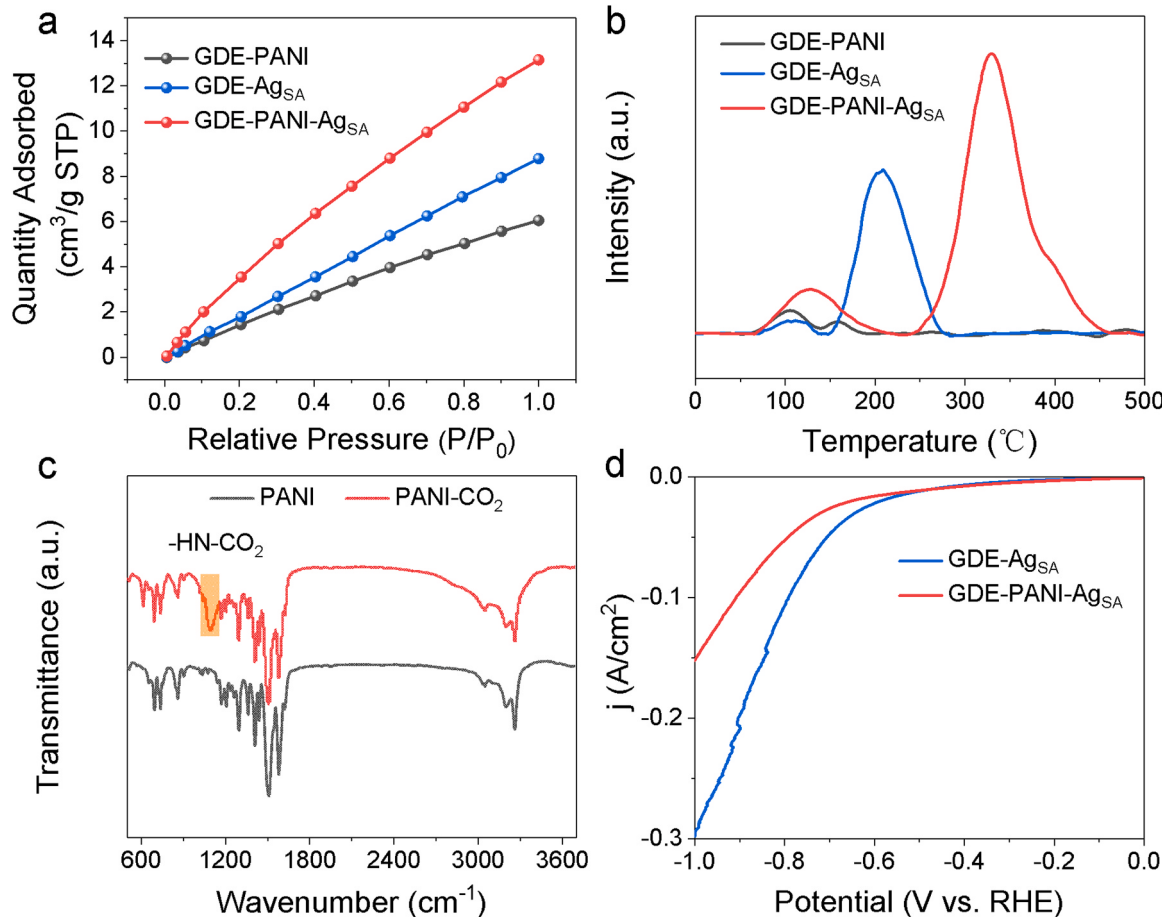


Fig. 5. (a) CO_2 adsorption isotherms of GDE-PANI, GDE-Ag_{SA} and GDE-PANI-Ag_{SA}. (b) CO_2 -TPD spectra of GDE-PANI, GDE-Ag_{SA} and GDE-PANI-Ag_{SA}. (c) FTIR spectra of PANI before and after interacting with CO_2 . (d) Electrochemical measurements for HER in 1 M KOH solution of GDE-Ag_{SA} and GDE-PANI-Ag_{SA}.

by activating CO₂ through the interactions between the basic amino group in PANI and the acidic CO₂ molecule, forming *COOH intermediate on the surface of Ag, thus favoring the efficient CO generation.

4. Conclusions

In summary, PANI-Ag_{SA} was successfully constructed on GDE via a simple in situ polymerization and reduction method. PANI prepared in neutral solution has more amino groups than that in acidic conditions. The amino group (–NH–) with strong electron donating ability could effectively promote the adsorption and activation of CO₂. The –NH– sites could also coordinate with Ag_{SA}, and the composite can readily convert CO₂ to CO. The optimized GDE-PANI-Ag_{SA} catalyst showed a relatively high CO₂RR activity and selectivity with a very low onset potential of –0.2 V (vs. RHE) with the FE_{CO} close to 100% at –0.75 V (vs. RHE) and a high energy efficiency of 12.8% in a flow cell system. The present work highlighted the cooperation of the active species and their chemical environments, shedding light on the importance for the in-depth understanding on structure-function relations for guiding and designing electrocatalysts to achieve efficient utilization of CO₂.

CRediT authorship contribution statement

Gaowu Qin: Writing – review & editing. **Teng Zhang:** Conceptualization, Data curation, Investigation, Software, Writing – original draft. **Song Li:** Funding acquisition, Validation, Writing – review & editing. **Xingyu Lu:** Validation, Writing – review & editing. **Wei Qi:** Funding acquisition, Validation, Writing – review & editing.

Declaration of Competing Interest

The authors declare that they have no known competing financial interests or personal relationships that could have appeared to influence the work reported in this paper.

Data availability

Data will be made available on request.

Acknowledgments

The authors acknowledge the financial support from the NSFC of China (22072163), the Natural Science Foundation of Liaoning Province of China (2020-YQ-02), China Baowu Low Carbon Metallurgy Innovation Foundation-BWLCF202113 and the Fundamental Research Funds for the Central Universities (N2202012).

Appendix A. Supporting information

Supplementary data associated with this article can be found in the online version at [doi:10.1016/j.apcatb.2024.123896](https://doi.org/10.1016/j.apcatb.2024.123896).

References

- [1] M. Reichstein, M. Bahn, P. Ciais, D. Frank, M.D. Mahecha, S.I. Seneviratne, J. Zscheischler, C. Beer, N. Buchmann, D.C. Frank, D. Papale, A. Rammig, P. Smith, K. Thonikke, M. Velde, S. Vicca, A. Walz, M. Wattenbach, Climate extremes and the carbon cycle, *Nature* 500 (2013) 287–295.
- [2] T.Y. Lei, D.P. Wang, X. Yu, S.J. Ma, W.C. Zhao, C. Cui, J. Meng, S. Tao, D.B. Guan, Global iron and steel plant CO₂ emissions and carbon-neutrality pathways, *Nature* 622 (2023) 514–520.
- [3] Y.Y. Birdja, E. Pérez-Gallent, M.C. Figueiredo, A.J. Göttle, F. Calle-Vallejo, M.T. M. Koper, Advances and challenges in understanding the electrocatalytic conversion of carbon dioxide to fuels, *Nat. Energy* 4 (2019) 732–745.
- [4] J.L. Qiao, Y.Y. Liu, F. Hong, J.J. Zhang, A review of catalysts for the electroreduction of carbon dioxide to produce low-carbon fuels, *Chem. Soc. Rev.* 43 (2014) 631–675.
- [5] X.Y. Dai, K. Qi, C.W. Liu, X.Y. Liu, W. Qi, Cooperative multifunctional nanocarbon as efficient electro-catalysts for CO₂ fixation to value-added cyclic carbonates under mild conditions, *Carbon* 202 (2023) 51–58.
- [6] P.D. Luna, C. Hahn, D. Higgins, S.A. Jaffer, T.F. Jaramillo, E.H. Sargent, What would it take for renewably powered electrosynthesis to displace petrochemical processes? *Science* 364 (2019) eaav3506.
- [7] H. Shin, K.U. Hansen, F. Jiao, Techno-economic assessment of low-temperature carbon dioxide electrolysis, *Nat. Sustain.* 4 (2021) 911–919.
- [8] X.J. Zhou, Y.Q. Liu, L. Liu, Y. Yu, J.A. Xu, M. Ruan, S. Li, L.H. Qian, Unveiling and utilizing the reconstructing dynamics on nanoporous Ag-Bi for CO₂ electroreduction, *Appl. Catal. B Environ.* 343 (2024) 123552.
- [9] F. Hu, S.C. Abeyweera, J. Yu, D.T. Zhang, Y. Wang, Q.M. Yan, Y.G. Sun, Quantifying electrocatalytic reduction of CO₂ on twin boundaries, *Chem* 6 (2020) 3007–3021.
- [10] C.M. Ye, S.J. Raaijman, X.T. Chen, M.T.M. Koper, Enhanced electrochemical CO₂ reduction to formate on poly(4-vinylpyridine)-modified copper and gold electrodes, *ACS Appl. Mater. Interfaces* 14 (2022) 45263–45271.
- [11] X.Y. Chen, J.F. Chen, N.M. Alghorabi, D.A. Henckel, R.X. Zhang, U.O. Nwabara, K. E. Madsen, P.J.A. Kenis, S.C. Zimmerman, A.A. Gewirth, Electrochemical CO₂-to-ethylene conversion on polyamine-incorporated Cu electrodes, *Nat. Catal.* 4 (2021) 20–27.
- [12] Y.B. Zou, T.X. Pan, Z.W. Fan, Y.B. Li, H. Zhang, Y. Ju, Y.F. Zhang, X.L. Ma, Q. H. Chen, S.C. Xiang, Z.J. Zhang, Ag-organic coordination polymers with multi-dimensional electron transfer channels for enhancing CO₂ electroreduction, *Chem. Eng. J.* 454 (2023) 140496.
- [13] X.Y. Dai, T.L. Cao, X.Y. Lu, Y.L. Bai, W. Qi, Tailored Pd/C bifunctional catalysts for styrene production under an ethylbenzene oxidative dehydrogenation assisted direct dehydrogenation scheme, *Appl. Catal. B Environ.* 324 (2023) 122205.
- [14] A. Vijayakumar, Y. Zhao, J.S. Zou, K.Z. Wang, C.Y. Lee, D.R. MacFarlane, C. Y. Wang, G.G. Wallace, A self-assembled CO₂ reduction electrocatalyst: posy-bouquet-shaped gold-polyaniline core-shell nanocomposite, *ChemSusChem* 13 (2020) 5023–5030.
- [15] X. Wei, Z.L. Yin, K.J. Lyu, Z. Li, J. Gong, G.W. Wang, L. Xiao, J.T. Lu, L. Zhuang, Highly selective reduction of CO₂ to C₂₊ hydrocarbons at copper/polyaniline interfaces, *ACS Catal.* 10 (2020) 4103–4111.
- [16] R. Sui, J.J. Pei, J.J. Fang, X.J. Zhang, Y.F. Zhang, F.J. Wei, W.X. Chen, Z. Hu, S. Hu, W. Zhu, Z.B. Zhuang, Engineering Ag-N_x single-atom sites on porous concave N-doped carbon for boosting CO₂ electroreduction, *ACS Appl. Mater. Interfaces* 13 (2021) 17736–17744.
- [17] A. Güngör, F. Bakan-Misirlioglu, R.G. Alturk, E. Erdem, Elevating supercapacitor performance: enhancing electrochemical efficiency with transition metal-doped polyaniline electrode, *J. Energy Storage* 76 (2024) 110143.
- [18] N. Parveen, N. Mahato, M.O. Ansari, M.H. Cho, Enhanced electrochemical behavior and hydrophobicity of crystalline polyaniline@graphene nanocomposite synthesized at elevated temperature, *Compos. Part B 87* (2016) 281–290.
- [19] X.J. Li, S.Y. Zhao, X.G. Duan, H.Y. Zhang, S.Z. Yang, P.P. Zhang, S.P. Jiang, S. M. Liu, H.Q. Sun, S.B. Wang, Coupling hydrothermal and photothermal single-atom catalysis toward excellent water splitting to hydrogen, *Appl. Catal. B Environ.* 283 (2021) 119660.
- [20] Y.J. Chen, S.F. Ji, C. Chen, Q. Peng, D.S. Wang, Y.D. Li, Single-atom catalysts: synthetic strategies and electrochemical applications, *Joule* 2 (2018) 1242–1264.
- [21] C. Hu, J.C. Hu, Z.J. Zhu, Y. Lu, S.Q. Chu, T.Y. Ma, Y.H. Zhang, H.W. Huang, Orthogonal charge transfer by precise positioning of silver single atoms and clusters on carbon nitride for efficient piezocatalytic pure water splitting, *Angew. Chem. Int. Ed.* 61 (2022) e202212397.
- [22] L.A. Ma, Q.H. Geng, L.L. Fan, J.X. Li, D.W. Du, J.L. Bai, C.L. Li, Enhanced electroreduction of CO₂ to C₂₊ fuels by the synergistic effect of polyaniline/CuO nanosheets hybrids, *Nano Res.* 16 (2023) 9065–9072.
- [23] Y.H. Yu, D. Wang, Y.M. Hong, T. Zhang, C.W. Liu, J. Chen, G.W. Qin, S. Li, Bulk-immiscible CuAg alloy nanorods prepared by phase transition from oxides for electrochemical CO₂ reduction, *Chem. Commun.* 58 (2022) 11163–11166.
- [24] N.Q. Zhang, X.X. Zhang, L. Tao, P. Jiang, C.L. Ye, R. Lin, Z.W. Huang, A. Li, D. W. Pang, H. Yan, Y. Wang, P. Xu, S.F. An, Q.H. Zhang, L.C. Liu, S.X. Du, X.D. Han, D.S. Wang, Y.D. Li, Silver single-atom catalyst for efficient electrochemical CO₂ reduction synthesized from thermal transformation and surface reconstruction, *Angew. Chem. Int. Ed.* 60 (2021) 6170–6176.
- [25] Y.B. Zou, T.T. Zhan, Y. Yang, Z.W. Fan, Y.B. Li, Y.F. Zhang, X.L. Ma, Q.H. Chen, S. C. Xiang, Z.J. Zhang, Single-phase proton-and-electron-conducting agorganic coordination polymers for efficient CO₂ electroreduction, *J. Mater. Chem. A* 10 (2022) 3216–3225.
- [26] Y.F. Li, C. Chen, R. Cao, Z.W. Pan, H. He, K.B. Zhou, Dual-atom Ag₂/graphene catalyst for efficient electroreduction of CO₂ to CO, *Appl. Catal. B Environ.* 268 (2020) 118747.
- [27] M. Li, Y. Hu, D.W. Wang, D.S. Geng, Enhanced electrochemical reduction of CO₂ to CO on Ag/SnO₂ by a synergistic effect of morphology and structural defects, *Chem. Asian J.* 16 (2021) 2694–2701.
- [28] H.Q. Fu, J.X. Liu, N.M. Bedford, Y. Wang, J.W. Sun, Y. Zou, M.Y. Dong, J. Wright, H. Diao, P. Liu, H.G. Yang, H.J. Zhao, Synergistic Cr₂O₃@Ag heterostructure enhanced electrocatalytic CO₂ reduction to CO, *Adv. Mater.* 34 (2022) 2202854.
- [29] T. Zhang, Y. Liu, C.C. Yang, L.M. Tian, Y.Y. Yan, G.Y. Wang, Monotonically increasing relationship between conversion selectivity from CO₂ to CO and the interface area of Cu-Ag biphasic electrochemical catalyst, *J. Alloy. Compd.* 947 (2023) 169638.
- [30] M. Luo, X.M. Fu, S. Geng, Z.W. Li, M. Li, Efficient electrochemical CO₂ reduction via CuAg doped CeO₂, *Fuel* 347 (2023) 128470.

[31] D. Ma, Y.R. Ying, K. Zhang, Y.L. Gao, L.J. Zhou, A. Song, Y.P. Zhu, K.Y. Xie, T. Jin, H.T. Huang, Greatly enhanced CO₂ electrocatalytic reduction performance of Ag₂Se nanocatalyst via phase-engineering, *Appl. Catal. B Environ.* 316 (2022) 121658.

[32] J.M. Chen, X.Q. Liu, S.B. Xi, T.Y. Zhang, Z.H. Liu, J.Y. Chen, L. Shen, S. Kawi, L. Wang, Functionalized Ag with thiol ligand to promote effective CO₂ electroreduction, *ACS Nano* 16 (2022) 13982–13991.

[33] Z. Zhang, G.B. Wen, D. Luo, B.H. Ren, Y.F. Zhu, R. Gao, H.Z. Dou, G.R. Sun, M. Feng, Z.Y. Bai, A.P. Yu, Z.W. Chen, “Two ships in a bottle” design for Zn–Ag–O catalyst enabling selective and long-lasting CO₂ electroreduction, *J. Am. Chem. Soc.* 143 (2021) 6855–6864.

[34] Y. Zhang, L. Chen, F.W. Li, C.D. Easton, J.Z. Li, A.M. Bond, J. Zhang, Direct detection of electron transfer reactions underpinning the tin-catalyzed electrochemical reduction of CO₂ using Fourier-transformed ac voltammetry, *ACS Catal.* 7 (2017) 4846–4853.

[35] T. Zhang, Y.H. Yu, C.W. Liu, G.W. Qin, S. Li, Constructing Ni₄W/WO₃/NF with strongly coupled interface for hydrogen evolution in alkaline media, *Rare Met.* 42 (2023) 3945–3951.

[36] M. Dunwell, W. Luc, Y.S. Yan, F. Jiao, B.J. Xu, Understanding surface-mediated electrochemical reactions: CO₂ reduction and beyond, *ACS Catal.* 8 (2018) 8121–8129.

[37] X.Y. Wang, Y.E. Jiang, K.K. Mao, W.B. Gong, D.L. Duan, J. Ma, Y. Zhong, J.W. Li, H.J. Liu, R. Long, Y.J. Xiong, Identifying an interfacial stabilizer for regeneration-free 300h electrochemical CO₂ reduction to C₂ products, *J. Am. Chem. Soc.* 144 (2022) 22759–22766.

[38] Y. Yang, S. Ajmal, Y.Q. Feng, K.J. Li, X.Z. Zheng, L.W. Zhang, Insight into the formation and transfer process of the first intermediate of CO₂ reduction over Ag-decorated dendritic Cu, *Chem. Eur. J.* 26 (2020) 4080–4089.

[39] W.Y. Shan, R. Liu, H.C. Zhao, Z.L. He, Y.J. Lai, S.S. Li, G.Z. He, J.F. Liu, In situ surface-enhanced raman spectroscopic evidence on the origin of selectivity in CO₂ electrocatalytic reduction, *ACS Nano* 14 (2020) 11363–11372.

[40] P.S. Li, J.H. Bi, J.Y. Liu, Y. Wang, X.C. Kang, X.F. Sun, J.L. Zhang, Z.M. Liu, Q. G. Zhu, B.X. Han, p-d Orbital hybridization induced by p-block metal-doped Cu promotes the formation of C₂₊ products in ampere-level CO₂ electroreduction, *J. Am. Chem. Soc.* 145 (2023) 4675–4682.

[41] P.A. Redhead, Thermal desorption of gases, *Vacuum* 12 (1962) 203–211.

[42] L. DeRita, J. Resasco, S. Dai, A. Boubnov, H.V. Thang, A.S. Hoffman, I. Ro, G. W. Graham, S.R. Bare, G. Pacchioni, X. Pan, P. Christopher, Structural evolution of atomically dispersed Pt catalysts dictates reactivity, *Nat. Mater.* 18 (2019) 746–751.

[43] G. Gregoire, N.R. Brinkmann, D.V. Heijnsbergen, H.F. Schaefer, M.A. Duncan, Infrared photodissociation spectroscopy of Mg⁺(CO₂)_n and Mg⁺(CO₂)_nAr clusters, *J. Phys. Chem. A* 107 (2003) 218–227.